Available online at www.sciencedirect.com
SCIENCE DIRECT®
Materials Chemistry and Physics 83 (2004) 307–314
MATERIALS CHEMISTRY AND PHYSICS
www.elsevier.com/locate/matchemphys

Electrochemical preparation and characteristics of Ni–Co–$LaNi_5$ composite coatings as electrode materials for hydrogen evolution

Gang Wu*, Ning Li, Chang Song Dai, De Rui Zhou

Department of Applied Chemistry, Harbin Institute of Technology, P.O. Box 411, Harbin 150001, PR China

Received 10 July 2003; received in revised form 9 September 2003; accepted 1 October 2003

Abstract

Electrocatalytic activity for the hydrogen evolution reaction on Ni–Co–$LaNi_5$ composite electrodes prepared by electrochemical codeposition technique was evaluated. The relationship between the current density for hydrogen evolution reaction and the amount of $LaNi_5$ particles in Ni–Co baths is like the well-known "volcano plot". The Surface morphology and microstructure of Ni–Co–$LaNi_5$ coatings were determined by means of scanning electron microscopy (SEM) and X-ray diffraction (XRD). The kinetic parameters were determined from electrochemical steady-state Tafel polarization and electrochemical impedance spectroscopy technology in 1 M NaOH solution. The values obtained for the apparent energies of activation are 32.48, 46.29 and 57.03 kJ mol^{-1} for the Ni–Co–$LaNi_5$, Ni–Co and Ni electrodes, respectively. The hydrogen evolution reaction on Ni–Co–$LaNi_5$ proceeds via Volmer–Tafel reaction route with the mixed rate determining characteristics. The composite coating Ni–Co–$LaNi_5$ is catalytically more active than Ni and Ni–Co electrodes due to the increase in its real surface areas and the decrease in the apparent free energy of activation caused by the electrocatalytic synergistic effect of the Ni–Co alloys and the hydrogen storage intermetallic particles on the electrode surface.

Keywords: Electrochemistry; Catalysis; Hydrogen; Composite coatings

1. Introduction

The electrocatalysis in the hydrogen evolution reaction is one of the most important subjects in electrochemistry. The study of this reaction has permitted the development of the fundamentals of the electrode kinetics as well as improving the technology of hydrogen production from water electrolysis. There are two properties playing important roles in selecting catalytically active materials for the hydrogen evolution reaction. One is the actual electrocatalytic effect of the materials, which is directly dependent on the voltage used to operate the electrolyzer at constant current density; the other is its long-term stability. Thus, from an electrochemical point of view, the problem to be tackled in order to decrease the cost of electrolytic hydrogen is the reduction of overpotentials. The desired decrease in overpotential can be achieved by choosing highly catalytically active electrode materials, or by increasing the active surface area of the electrode. The intrinsic activity depends on the density of active site on the surface, which is controlled by the electronic structure of the material. This structure can be changed by alloying. Miao and Piron [1] observed that Ni, Co, Fe alloy prepared by electrolytic codeposition were catalytically more active for hydrogen evolution reaction than Ni electrode deposited under the same condition. The alloying effect of transition metal-based alloys on hydrogen evolution has been discussed on the basis of the Engel–Brewer valence-bond theory [2,3]. In the Engel–Brewer theory, the strong bonding is considered to be achieved by filling the vacant d-orbitals of the early transition metals with the electrons donated from non-bonding orbitals of the late transition metals, which results in the formation of stable intermetallic compounds. Electrodeposition technologies for obtaining electrode materials have many characteristics enabling a controlling influence to be exerted over the chemical and phase composition and also on the surface morphology of the coatings [4–6]. There are also possibilities for utilizing the ability to incorporate suspended particles from the galvanic bath into the structure of the alloy layer by composite electrodeposition method, and the formation of composite coatings have high electrocatalytic activity resulting from larger real surface areas of the electrodes [7]. Furthermore, the electrochemical codeposition process of particles and metallic ions has helped to achieve the synergetic effect of

* Corresponding author. Tel.: +86-451-86413721; fax: +86-451-86221048.
E-mail address: wugang1976@hotmail.com (G. Wu).

0254-0584/$ – see front matter © 2003 Elsevier B.V. All rights reserved.
doi:10.1016/j.matchemphys.2003.10.005

both species for electrocatalytic performance. Electrode materials such as Ni–MoS_x, Ni–FeS and Ni–RuO_2, can be cited as evidence of success of the codeposition process in obtaining hydrogen evolution reaction electrocatalysts [8–11].

Some hydrogen storage alloys were found to have a high electrocatalytic activity for hydrogen evolution in alkaline media, almost comparable to Pt and Pd electrodes. Tanaka et al. [12] reported apparent exchange current density ($\log j_0$/A cm^{-2}) equal to −3.5 for $LaNi_5$, which is similar to the values obtained for Pd (−3.9) and Pt (−3.5). Machida and Enyo [13] published that $LaNi_5$ and other combinations of rare-earth metals and Ni, used as cathode come close to the reversible hydrogen electrode over a wide range of current densities. The authors highlighted the good performance of the electrode materials and proposed that the hydrogen evolution reaction on the $LaNi_5$ alloys proceeds via the Volmer–Tafel reaction route with mixed rate determining characteristics. However, the hydrogen storage alloy electrodes such as $LaNi_5$ are liable to sustain damage owing to hydrogen embrittlement during cathodization [14]. The codeposition process of hydrogen storage alloy and Ni can give the electrode material the desirable characteristics of mechanical resistance and electrocatalytic activity. Bocutti et al. [15] investigated kinetic and mechanistic parameters for the hydrogen evolution reaction on Ni/$LaNi_5$ codeposits in alkaline medium.

At present, though the most important electrode materials are nickel and its alloys, nickel electrode is not very stable and its activity decrease progressively with time. Comparing with nickel electrode, the nickel–cobalt alloy has better electrocatalytic activity and the long-term stability to tolerance to electrochemical corrosion in electrolyte [16].

The aim of this work was to prepare the composite coatings based on Ni–Co alloy matrix containing $LaNi_5$ particles, to determine their structure and chemical composition and also to evaluate their suitability as Electrocatalytic materials for hydrogen evolution reaction in an alkaline medium.

2. Experimental details

In order to obtain electrolytic composite Ni–Co–$LaNi_5$ coatings, an electrolyte for Ni–Co codeposition was prepared to have the following composition: 0.8 M $Ni(NH_2SO_3)_2{\cdot}4H_2O$, 0.2 M $Co(NH_2SO_3)_2{\cdot}4H_2O$, 0.1 M H_3BO_3 and 0.2 M NaCl, to which 1–9 g l^{-1} $LaNi_5$ particles was added. From these electrolytes, the Ni–Co–$LaNi_5$ composite coatings with about 30 wt.% Co and different $LaNi_5$ content can be obtained. Been observed by an optical microscope, the mean size of the $LaNi_5$ particles was estimated to be 2 μm. Reagents of analytical purity and double distilled water were used for the solutions. pH of the suspension was equal to about 4.0–4.5. The composite coatings were electrodeposited on copper substrates (only used for Lab studying), which the one side geometric area was 10 cm^2. The process was carried out at a temperature 50 °C with intensive mechanical stirring (300 rpm) to maintain the particles in suspension. Electrolytic composite Ni–Co–$LaNi_5$ coatings were obtained under galvanostatic conditions, at the current density of 50 mA cm^{-2}. In order to evaluate the influence of $LaNi_5$ particles on electrocatalytic activity, Ni–Co and Ni coatings were also obtained under the same conditions from a bath without particles and comparative tests were conducted on them.

Surface morphology of the Ni–Co–$LaNi_5$, Ni–Co and Ni coatings was determined by the means of scanning electron microscopy (SEM). The electrodeposited composite coatings were measured by X-ray diffractograms recorded by a Bede D1 diffractometer, starting from 2θ starting from 20° to 100° in 0.05° and 1s steps. The Cu Kα ray ($\lambda = 0.15418$ nm) was selected through a graphite monochromator. To determine the percentage composition of the electrodeposited alloys, the deposits were stripped in a 1:3 HNO_3 solution and diluted with distilled water and analyzed for Ni, Co and La using an Atomic adsorption (AAS) and then calculated $LaNi_5$ particles content.

All electrochemical measurements were performed in a two-compartment electrochemical cell. The experiments were carried out in 1 M NaOH solution at a temperature range from 20 to 60 °C. A large area platinum sheet was used as the counter electrode and the Hg/HgO, NaOH 1 M solution was used as the reference electrode. Oxygen was removed from the solution by bubbling nitrogen gas (99.99%). Steady-state polarization curves were performed using an EG&G PAR 273 Potentiostat-Galvanostat controlled by an IBM compatible PC. All the steady-state overpotential values were *jR* corrected from the resistance value, estimated from electrochemical impedance spectroscopy (EIS) experiments. The EIS experiments were carried out in a frequency range from 10 kHz to 0.01 Hz (r.m.s. amplitude = 5 mV), maintaining each potential on the electrode for 30 min before starting data acquisition. During the experiments nitrogen gas was passed over the electrolytic solution. An EG&G PARC 1025 Frequency Response Detector was used for these measurements.

3. Results and discussion

3.1. The codeposition of Co–Ni/$LaNi_5$ coatings

Fig. 1 shows the relationship between concentration of $LaNi_5$ particles in the electrolyte and content of $LaNi_5$ in deposit. It can be noted that $LaNi_5$ in the deposit increases with an increase of $LaNi_5$ in the bath, tending to attain a steady value at $LaNi_5$ concentration of 5 g l^{-1}.

Moreover, the curves are quite similar to the well-known Langmuir adsorption isotherms, supporting a mechanism based on an adsorption effect. Once the particle is adsorbed, metal begins building around the cathode slowly, encapsulating and incorporating the particles. The plateau observed

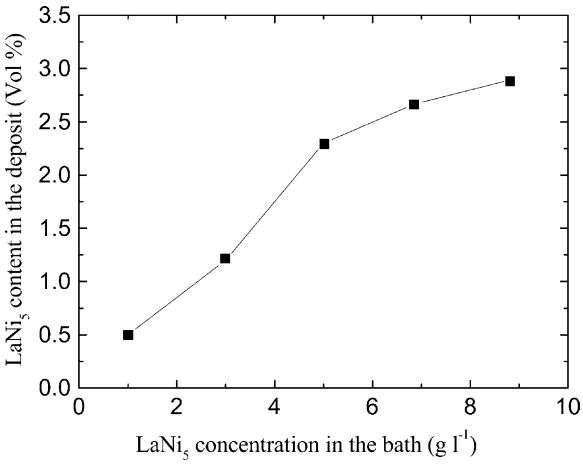

Fig. 1. Relationship between $LaNi_5$ concentration in bath and $LaNi_5$ content in deposit, $j_k = 3\,A\,dm^{-2}$, pH 4.5, 300 rpm.

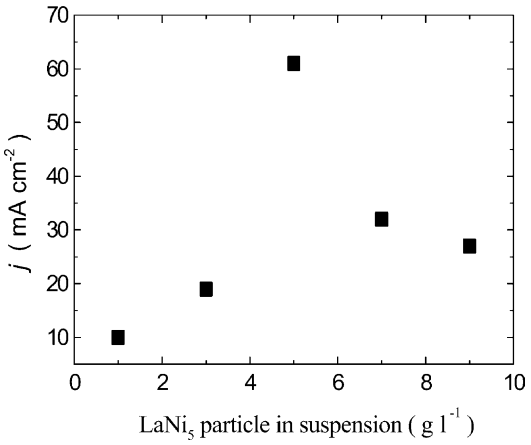

Fig. 2. The current density for hydrogen evolution at overpotential, $\eta = 0.4\,V$, measured in $1.0\,mol\,l^{-1}$ NaOH at 20 °C for the Ni–Co–$LaNi_5$ coatings electrodeposited from Ni–Co baths containing different amount of $LaNi_5$.

at higher particles concentration in bath may be a result of saturation in adsorption on cathode surface.

3.2. The effect of $LaNi_5$ content on hydrogen evolution reaction

In Fig. 2 the current density for hydrogen evolution reaction at overpotential, $\eta = 0.4\,V$, measured in $1.0\,mol\,l^{-1}$ NaOH at 20 °C on Ni–Co–$LaNi_5$ electrode was plotted vs. the different amount of $LaNi_5$ particles in Ni–Co electrolytes to prepare Ni–Co–$LaNi_5$ composite coatings. This plot is like the well-known "volcano plot" for the hydrogen evolution on different metals [17]. As can be seen a maximum current density of $62\,mA\,cm^{-2}$ at overpotential, $\eta = 0.4\,V$ for hydrogen evolution reaction was obtained on Ni–Co–$LaNi_5$ composite coating which prepared from electrolyte containing $5\,g\,l^{-1}$ $LaNi_5$ particles. The volcano plot found for hydrogen evolution reaction on Ni–Co–$LaNi_5$ composite coatings could have a similar explanation. The binding energy between the adsorbed hydrogen and the coatings could depend on the electronic structure of the coatings, and this structure is influenced by the content of $LaNi_5$ in composite coatings.

So far as our present work, we just reported the results of the Ni–Co–$LaNi_5$ electrode obtained from the electrolyte containing $5\,g\,l^{-1}$ $LaNi_5$ particles.

3.3. Electrode morphology and surface structure

Electrolytic composite coatings Ni–Co–$LaNi_5$ exhibited good adhesion to the substrate and no internal stress causing their detachment were observed. Fig. 3 shows the comparison of the SEM morphology of Ni–Co–$LaNi_5$, Ni–Co alloys and Ni coatings. It can be seen that the Ni–Co deposit has a rather regular fibril surface, whereas the Ni–Co–$LaNi_5$ composite coating develops a nodular surface structure. A coarser grain size is observed in the composite coatings compared to the Ni–Co deposits. Due to electrical conductivity of $LaNi_5$ particles, the metal ions can directly deposit on the particle surface. So the larger grain of Ni–Co alloys was attributed to an increase in the active surface area and a decrease in cathodic polarization due to the adsorbed particles on the cathode surface. The heterogeneity of $LaNi_5$ particles and Ni–Co matrix increases the real surface area and interface number between Ni–Co and in-

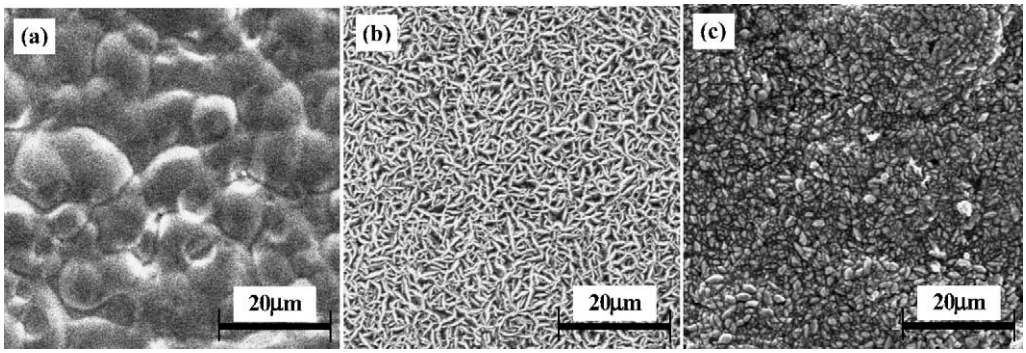

Fig. 3. Scanning electron micrographs of the electrode materials. (▲) f.c.c. Ni, (●) f.c.c. Co, (■) $LaNi_5$. (a) Ni; (b) Ni–30Co; (c) Ni–30Co–$LaNi_5$.

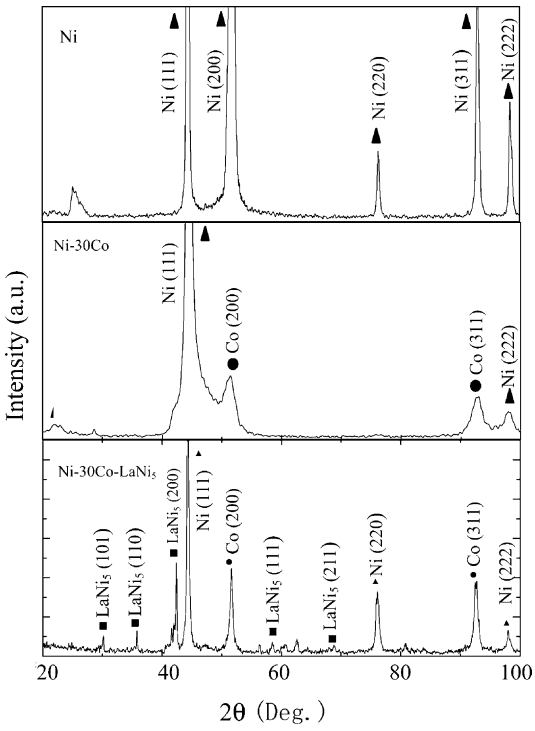

Fig. 4. XRD patterns of the electrode materials.

corporated particles. Such electrode surface contributes to improve the electrocatalytic activity of hydrogen evolution reaction.

X-ray diffraction patterns corresponding to the Ni, Ni–Co and Ni–Co–$LaNi_5$ coatings, respectively, are shown in Fig. 4. Pure Ni coating exists the reflections (1 1 1), (2 0 0), (2 2 0), (3 1 1) and (2 2 2), which belong to the f.c.c. structure of nickel. Ni–30Co alloy also shows f.c.c. nickel and f.c.c. cobalt phase structure and Ni–Co–$LaNi_5$ have a multiphase structure which beside the peaks of f.c.c. nickel and f.c.c. cobalt phase structure, the reflections (1 0 1), (1 1 0), (2 0 0), (1 1 1) and (2 1 1) belonged to the $LaNi_5$ structure are observed.

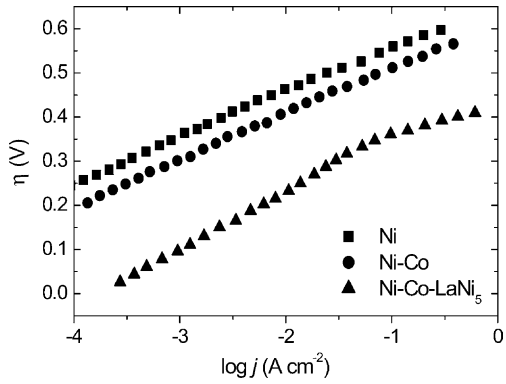

Fig. 5. Tafel plots obtained for hydrogen evolution reaction on the three studied electrode materials in 1 M NaOH at 20 °C.

3.4. Polarization measurements

Fig. 5 shows the Tafel plots and polarization data for hydrogen evolution reaction on the three investigated electrodes built from steady state, *jR* corrected. The activity of these coatings toward the hydrogen evolution reaction was analyzed in the temperature range of 20–60 °C. The corresponding Tafel parameters including exchange current density j_0, Tafel slope b_c, cathodic overpotential η, at different temperatures are listed in Table 1. The data obtained from the steady-state polarization experiment have shown pronounced improvement in the catalytic performance for hydrogen evolution reaction on the codeposited Ni–Co–$LaNi_5$ electrode, with respect to the Ni and Ni–Co electrodes. Compared with Ni electrode, such improvement is characterized by a 30 times increase of the apparent exchange current density and by a nearly 150 mV decrease in the overpotential value for a current density of 250 mA cm^{-2} (η_{250}) at the temperature of 20 °C. The experimental Tafel slope observed at low overpotential on Ni–Co–$LaNi_5$ electrode is about 120 mV dec^{-1} and slight higher than that of Ni and Ni–Co electrodes. However, at high overpotential, Tafel slope of Ni–Co–$LaNi_5$ is closed to 39 mV dec^{-1} and lower than that of Ni and Ni–Co electrodes.

Table 1
Tafel parameters for the hydrogen evolution reaction on the studied electrode materials in 1 M NaOH

Electrode	T (°C)	b_c (mV dec^{-1})		j_0 ($\times 10^5$ A cm^{-2})	η_{250} (V)	Roughness factor	$\Delta G^{\neq}$ (kJ mol^{-1})
		Low η	High η				
Ni	20	0.112		0.02	0.579		
	40	0.109		0.08	0.560	6	57.03
	60	0.124		0.34	0.534		
Ni–30Co	20	0.117		0.10	0.542		
	40	0.114		0.39	0.513	15	46.29
	60	0.123		0.95	0.495		
Ni–30Co–$LaNi_5$	20	0.121	0.037	0.60	0.420		
	40	0.129	0.034	1.41	0.390	236	32.48
	60	0.135	0.036	3.20	0.373		

It is widely accepted that hydrogen evolution reaction in alkaline solution goes through these steps:

$$H_2O + M + e^- \leftrightarrow MH_{ads} + OH^- \quad \text{(Volmer step)} \quad (1)$$

$$MH_{ads} + H_2O + e^- \leftrightarrow M + H_2 + OH^- \quad \text{(Heyrovsky step)} \quad (2)$$

$$MH_{ads} + MH_{ads} \leftrightarrow 2M + H_2 \quad \text{(Tafel step)} \quad (3)$$

MH_{ads} symbolizes the hydrogen adsorbed on the active site of the electrode surface. For hydrogen storage materials, a hydrogen diffusion process form the surface to the near surface bulk layer must be added:

$$MH_{ads} \leftrightarrow MH_{abs} \quad \text{(Absorption step)} \quad (4)$$

In Fig. 5 Ni–Co–$LaNi_5$ electrode shows different Tafel slopes at different overpotential regions. Due to the favorable hydrogen adsorption properties of $LaNi_5$ particles, at the low overpotential region, the Tafel slope of Ni–Co–$LaNi_5$ electrode is closed to 120 mV dec^{-1} and represent the overpotential component for a one electron transfer reaction, namely the Volmer step is rate determine step (rds). However, at the high overpotential, it is seen that Tafel slope of Ni–Co–$LaNi_5$ is about 39 mV dec^{-1}, and rds may be attributed to the Tafel step [13]. According to the research results of Gennero and Chialvo [18], the Tafel curves of Ni–Co–$LaNi_5$ electrode are consonant to the Volmer–Tafel mechanism. The hydrogen evolution reaction on the Ni–Co–$LaNi_5$ electrode is thus composed of the Volmer and Tafel elementary steps. In term of the result of Enyo [19], at the low overpotentials j_0 certainly represents the electrocatalytic activity of the electrode.

According to the Arrhenius relation:

$$\log j_0' = \log(FKc) - \frac{\Delta G^{\neq}}{2.3RT} \quad (5)$$

where j_0' is the real exchange current density, K the constant, c the concentration of reactant, T the absolute temperature, F the Faraday constant, R the gas constant, $\Delta G^{\neq}$ the apparent energy of activation. The linear relations between $\log j_0'$ and $1/T$ for each electrode material are displayed in Fig. 6 and allow the calculation of apparent energy of activation ($\Delta G^{\neq}$) for the hydrogen evolution reaction. The value obtained for the Ni–Co–$LaNi_5$ (32.48 kJ mol^{-1}) is smaller than the Ni–Co (46.29 kJ mol^{-1}) and Ni (57.03 kJ mol^{-1}), which is similar to those reported by Correia and Sergio[20] for Ni–Co (41 kJ mol^{-1}) and for Co (59 kJ mol^{-1}). Because of the difference in apparent energy of activation of three electrode materials, it must be pointed out that such an improvement in the electrocatalytic performance of the Ni–Co–$LaNi_5$ electrode materials could not be exclusively assigned to the increase of the electroactive surface area. It can be proposed that the occlusion of the hydrogen storage alloy particles in the electrode surface has provided desirable electrocatalytic activity.

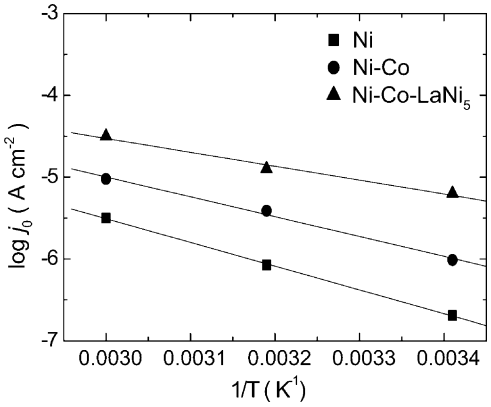

Fig. 6. The logarithm of exchange current density for different electrode materials as a function of the $1/T$, based on the real electrode surface.

3.5. Impedance spectroscopy measurements

Wide frequency range impedance measurements were further carried out to investigate the interfacial properties and kinetics of the hydrogen evolution reaction on Ni–Co–$LaNi_5$ electrode in comparison with pure Ni and Ni–Co electrodes.

The results obtained for three electrodes are presented in Bode plots ($\log|Z|$ and phase angle vs. $\log f$ in Fig. 7). For three electrode materials, between $\eta = 0.05$ and 0.45 V. At intermediate frequencies a linear dependence of $\log|Z|$ against $\log f$ and one well-defined maximum in the phase angle against $\log f$ plots were observed. The maximum is overpotential and frequency-dependent and its appearance indicates capacitive behavior of the electrode. At low and high frequencies, a transition from capacitive to resistive behavior is apparent. The phase angle θ, drop towards zero at both high and low frequencies, is attributed to resistive behavior of the electrode–electrolyte resistance R_{el}, and Faradaic resistance ($R_{el} + R_{ct}$), respectively. The ohmic resistance is the dominating impedance component at highest frequencies and the value of electrolyte resistance, R_{el}, can be deduced from the high frequency impedance plateau. At the lowest frequencies, the Faradaic resistance, i.e. the charge transfer resistance, R_{ct} dominates, which can be obtained from the low frequencies impedance plateau as ($R_{el} + R_{ct}$).

It should be noted that the modulus of the overall low frequency impedance $|Z|$, reaches its maximum. The maximum continuously decreases with increasing overpotential. The $|Z|$ values of charge transfer resistance on Ni–Co–$LaNi_5$ electrode are very low, and a few orders of magnitude lower than the Ni and Ni–Co electrodes.

Fig. 8 shows the complex-plane impedance diagrams (Nyquist plot) at $\eta = 0.45$ V on three electrode materials. The impedance spectra consist of two overlapping semicircles. The experimental data are treated through the complex non-linear least squares (CNLLS) fitting to estimate the elements of the Armstrong's equivalent circuit given in

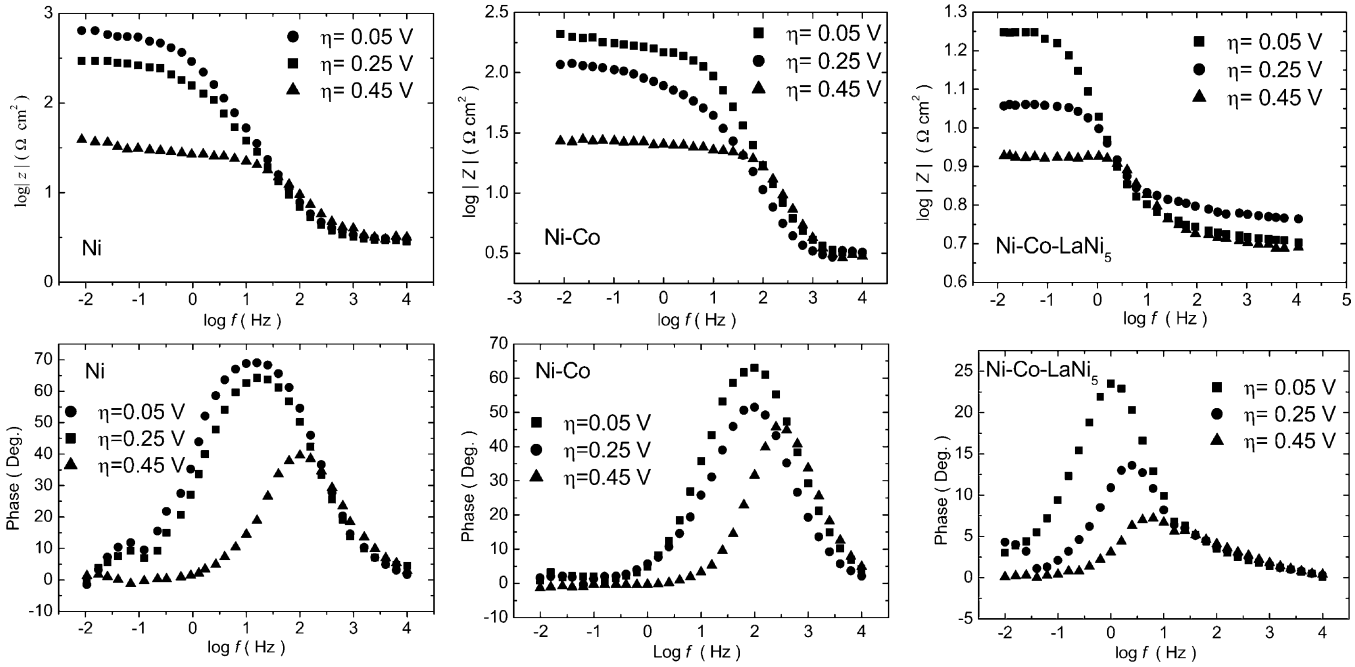

Fig. 7. Impedance spectra (Bode plots) of electrodes for hydrogen evolution reaction at 20 °C and various overpotentials.

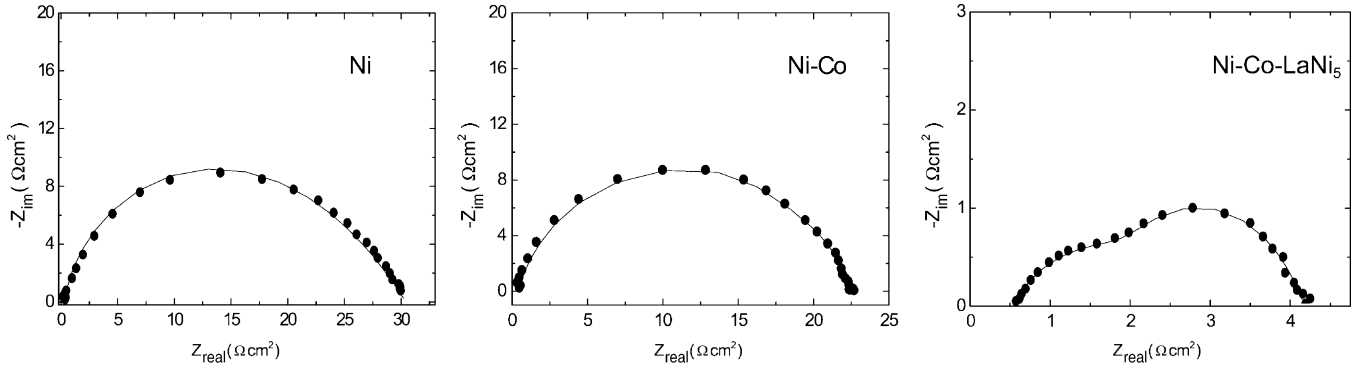

Fig. 8. Complex plane impedance plots for hydrogen evolution reaction on different electrode materials at 20 °C and $\eta = 0.45$ V. Experimental (circled points) and fitted result (solid lines) from equivalent circuit given in Fig. 9.

Fig. 9 [21,22]. The adopted model permits kinetic parameters such as C_{dl}, R_{ct}, R_P, C_P to be obtained, where C_{dl} is the electrode double-layer capacitance, R_{ct} is the charge transfer resistance for the electrode reaction, R_P is the basically related to the mass transfer resistance of the adsorbed intermediate H_{ads}, usually called the pseudo-resistance, and C_P is the pseudo-capacitance.

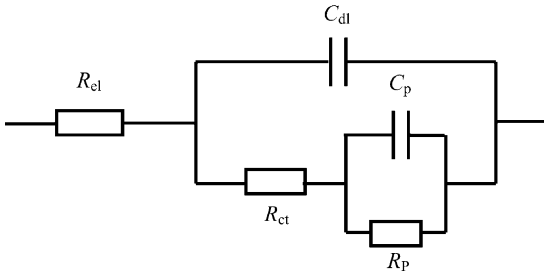

Fig. 9. Electrical equivalent circuit used for simulating the ac impedance spectra for the hydrogen evolution reaction on electrodes.

For the Armstrong equivalent electric circuit the Faradaic impedance, Z_f is defined as follows:

$$Z_f = R_{ct} + \frac{R_P}{1 + j\omega\tau_P} \quad (6)$$

where ω is the frequency and $\tau_P = R_P C_P$ is a time constant related to the relaxation rate of the electrode when its potential is changed [24]. The value of the impedance parameters are determined by CNLLS fitting procedure and listed in Table 2.

For lower electrode overpotentials the hydrogen absorbing electrode materials Ni–Co–$LaNi_5$ present pronouncedly higher C_{dl} values in relation to the pure electrodeposited Ni and Ni–Co, the hydrogen storage intermetallic particles might present microfissures and increase the real area of

Table 2
The fitted parameters values of the equivalent for hydrogen evolution reaction on different electrodes at 20 °C

Electrode	η (V)	R_{ct} ($\Omega\,cm^{-2}$)	C_{dl} ($\mu F\,cm^{-2}$)	R_P ($\Omega\,cm^{-2}$)	C_P ($\mu F\,cm^{-2}$)	j_0 ($\times 10^5\,A\,cm^{-2}$)
Ni	0.05	1077	171	632	1589	
	0.25	544.3	163	226.3	2802	0.5
	0.45	24.0	126	12.3	8368	
Ni–30Co	0.05	125.3	380	49.5	3830	
	0.25	41.0	329	27.7	5466	1.4
	0.45	20.1	305	2.36	8158	
Ni–30Co–$LaNi_5$	0.05	13.3	4757	11.6	3609	
	0.25	5.7	4997	2.0	5317	31.6
	0.45	3.3	4728	1.2	7182	

electrode surface. In order to compare the real catalytic activity of different electrodes, their surface area must first be assessed and the surface effect should be subtracted from the apparent activity. The surface roughness factor of the electrodes, proportional to their electrochemically active surface area, was evaluated based on the apparent double-layer capacitances, C_{dl}, determined by impedance measurements. The surface roughness factor σ for each electrode was calculated by dividing C_{dl} by the double-layer capacitance ($20\,\mu F\,cm^{-2}$) of a smooth metal surface [23]. The surface roughness factor determined by impedance measurements was about 6 for Ni electrode, 15 for Ni–Co electrode and 236 for Ni–Co–$LaNi_5$ electrode.

With known values of charge transfer resistance, it is possible to calculate the exchange current density j_0, according to the relation [25]:

$$\left(\frac{\partial\eta}{\partial j}\right)_{\eta=0} = \frac{RT}{ZF}\frac{1}{j_0} = R_{ct} \tag{7}$$

The dependence of the logarithm of the charge transfer resistance on the overpotential, recalculated for the real surface area, is presented in Fig. 10. From this figure, it may be pointed out that in the overpotential range from -0.05 to -0.45 V, the relationship between $\log R_{ct}^{-1}$ and η is linear with $d\eta/d(\log R_{ct}^{-1})$ of 100 mV dec^{-1} for Ni, 119 mV dec^{-1} for Ni–Co and 128 mV dec^{-1} for Ni–Co–$LaNi_5$. The slopes almost close to the Tafel slopes obtained at low overpotential (0.05–0.3 V). Extrapolating the values of charge transfer resistance to the zero overpotential, according to Eq. (7), yields the exchange current densities j_0 for the hydrogen evolution reaction [26]. Thus based on the real surface areas the value of the exchange current densities are $31.6 \times 10^{-5}\,A\,cm^{-2}$ for Ni–Co–$LaNi_5$, $1.4 \times 10^{-5}\,A\,cm^{-2}$ for Ni–Co and $0.5 \times 10^{-5}\,A\,cm^{-2}$ for Ni electrode.

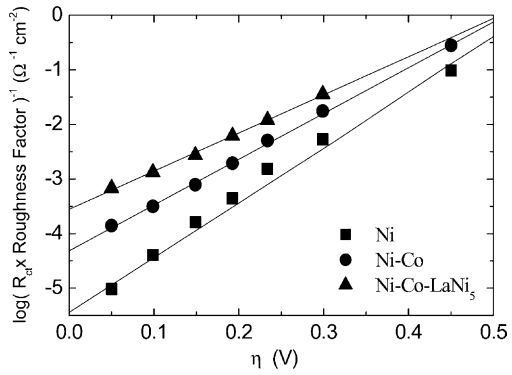

Fig. 10. The logarithm of charge transfer admittance, $\log(R_{ct}^{-1})$ for hydrogen evolution reaction on electrode as a function of the overpotential, based on the real electrode surface.

The strength of the H_2O–M and H–M interactions seems to be very important in discussions about surface electrocatalytic effect. In the hydrogen evolution reaction mechanism, the H_2O–M interaction should be strong enough to favor the splitting of the water molecule; conversely, the H–M interaction should not be so strong as to favor hydrogen desorption. In fact, it can be seen from the well-known electrocatalytic "volcano plots" for the hydrogen evolution reaction on the transitional metal, that Pt and Pd exhibit maximum electrocatalytic activity because of their intermediate M–H bonding strength. With this assumption, it can be accepted that the Volmer step should be the rds due to its high-energy requirement in the adsorption and splitting of the water molecule. As the above discussion, the hydrogen evolution reaction of the Ni–Co–$LaNi_5$ electrode consists on the Volmer reaction and subsequently Tafel reaction. Due to the incorporation of $LaNi_5$ particles into Ni–Co alloys, the hydrogen storage alloys enhance the H adsorption on the electrode surface. So the Ni–Co–$LaNi_5$ electrode has an intermediate M–H bonding strength and results in the improved electrocatalytic activity for hydrogen evolution reaction. Meanwhile, the Engel–Brewer valence bond theory should be used to consider the electrocatalytic activity of the employed particles [27]. For hydrogen evolution reaction, the Volmer step (the discharge of water molecules) needs paired d-orbital electrons, for instance, Ni d-orbital, to facilitate electron transfer to the water molecule and subsequent cleavage of the O–H bond. For the next step to succeed, semi-empty d-orbitals must be available, for instance, La and Co d-orbitals, to facilitate the M–H adsorption step. From this point of view, the electrocatalytic effect observed for hydrogen evolution reaction on Ni–Co–$LaNi_5$ surfaces should be enhanced by the appropriate combi-

nation of d^8-orbitals of Ni with d^1-orbitals of La and d^7-orbitals of Co. Volmer step was improved pronouncedly due to the availability of La and Co semi-empty d-orbitals, which facilitates splitting of the water molecule and MH_{ads} formation.

4. Conclusion

Electrocatalytic activity for the hydrogen evolution reaction on Ni–Co–$LaNi_5$, Ni–Co and Ni electrodes prepared by electrochemical codeposition technique was evaluated. The relationship between the current density for hydrogen evolution reaction and the amount of $LaNi_5$ particles in Ni–Co electrolytes is like the well-known "volcano plot". A maximum current density can be obtained at $5\,g\,l^{-1}$ $LaNi_5$ in bath. The real kinetic parameters (j_0, R_{ct}, b_c, η) were determined from apparent experimental results taking into account the roughness factor. The exchange current densities per true unit surface area were obtained from non-linear lease square fit of the impedance data and are consistent with the results obtained from the analysis of polarization curves. The apparent energy of activation values for the hydrogen evolution reaction are 32.48, 46.29 and $57.03\,kJ\,mol^{-1}$ on Ni–Co–$LaNi_5$, Ni–Co and Ni electrodes, respectively. The increase in electrocatalytic activity of the composite electrode Ni–Co–$LaNi_5$ for hydrogen evolution reaction may be mainly attributed to the increase in its real surface areas and the decrease in the apparent free energy of activation caused by electrocatalytic synergistic effect of the Ni–Co alloys and the hydrogen storage intermetallic $LaNi_5$ particles on the electrode surface.

The hydrogen evolution reaction on Ni–Co–$LaNi_5$ proceeds via Volmer–Tafel reaction route. At the low overpotential, the Volmer step was rate determine step, while with the increasing of overpotential, Tafel step became rate determine step. The observed improvement of hydrogen evolution reaction on Ni–Co–$LaNi_5$ electrode was discussed in the light of the Engel—Brewer valence bond theory, thus the rare-earth metal semi-empty d-orbitals facilitates splitting of the water molecule and MH_{ads} formation.

Acknowledgements

This work was financially supported by the High-New Technique Development Project of ShanDong province, China.

References

[1] H.J. Miao, D.L. Piron, Electrochim. Acta 39 (1994) 2715.
[2] M.M. Jaksic, Electrochim. Acta 29 (1984) 1539.
[3] M.M. Jaksic, Electrochim. Acta 39 (1994) 1695.
[4] A.C. Tavares, S. Trasatti, Electrochim. Acta 45 (2000) 4195.
[5] C. Fan, D.L. Poiron, Surf. Coat. Technol. 73 (1995) 91.
[6] J. Surowka, A. Budniok, B. Bzowshi, Thin Solid Films 307 (1997) 233.
[7] M. Keddam, S. Senyarich, H. Takenouti, P. Bernard, J. Appl. Electrochem. 24 (1994) 1037.
[8] L.B. Albertini, A.C.D. Angelo, E. Gonzalez, J. Appl. Electrochem. 22 (1992) 888.
[9] N.A. Assuncao, M.D. Giz, G. Tremiliosi, E. Gonzalez, J. Electrochem. Soc. 144 (1997) 2794.
[10] A.C. Tavares, S. Trasatti, Electrochim. Acta 45 (2000) 4195.
[11] C. Iwakura, M. Tanaka, S. Nakamatsl, H. Inoue, Electrochim. Acta 40 (1995) 977.
[12] M. Tanaka, S. Nakamatsu, M. Matsuoka, N. Furukawa, C. Iwakura, Denki Kagaku 61 (1993) 790.
[13] K. Machida, M. Enyo, Electrochim. Acta 29 (1984) 1723.
[14] T. Kitamura, C. Iwakura, H. Tamura, Electrochim. Acta 27 (1982) 1723.
[15] R. Bocutti, M.J. Saeki, A.O. Florention, C.L.F. Oliveira, A.C.D. Angelo, Int. J. Hydrogen Energy 25 (2000) 1051.
[16] I.A. Raj, K.I. Vasu, J. Appl. Electrochem. 20 (1990) 32.
[17] R. Parsons, Trans. Faraday Soc. 54 (1958) 1053.
[18] M.R. Gennero, A.C. Chialvo, Electrochim. Acta 44 (1998) 841.
[19] M. Enyo, Electrochim. Acta 18 (1973) 155.
[20] N.A. Correia, A.S. Sergio, A.L. Avaca, Electrochem. Commun. 1 (1999) 600.
[21] J.R. Macdonald, J. Schoonman, A.P. Leher, J. Electroanal. Chem. 131 (1982) 77.
[22] B.A. Boukamp, Solid State Ionics 20 (1980) 3.
[23] A. Jukic, J. Piljac, M.M. Hukovic, J. Mol. Catal. A 166 (2001) 293.
[24] N. Krstajic, M. Popovic, B. Grgur, M. Vojnovic, Electroanal. Chem. 512 (2001) 16.
[25] R.K. Shervedani, A. Lasia, J. Appl. Electrochem. 29 (1999) 979.
[26] M.M. Hukovic, A. Jukic, Electrochim. Acta 45 (2000) 4159.
[27] M.M. Jaksic, J. Mol. Catal. 38 (1986) 161.